AIAA JOURNAL
Vol. 41, No. 3, March 2003

Probe to Measure Direction and Strength of Moving Shocks or Blast Waves

Yiannis Andreopoulos,* Minwei Gong,† Zhexuan Wang,† and Savvas Xanthos†
City College of the City University of New York, New York, New York 10031

A new probe, capable of detecting the local direction of blast or moving shock waves and their strength, has been designed, fabricated, and tested. The performance of the probe has been assessed and validated in shock-tube tests, as well as in field measurements. The data obtained were also compared with computational fluid dynamics calculations with satisfactory results. The probe is sensitive to the incoming shock and flow direction. Its directional response is, to a certain extent, similar to that of a single pressure transducer. However, the ability to determine the shock wave direction provides better estimates of the pressure measurements behind the shock. In that respect, the present probe maybe characterized as omnidirectional. Evaluation tests of the algorithm developed to detect the direction and strength of blast waves indicated that the direction could be estimated within 5 deg of the true direction. The pressure behind the shock could be determined subsequently by several methods within a 10% uncertainty.

Nomenclature

M_s	=	shock wave Mach number
$\boldsymbol{n}_p$	=	unit vector normal to probe's sensing area
$\boldsymbol{n}_u$	=	unit vector in the velocity direction
p_m	=	measured pressure after passing of reflected shock wave
p_{refl}, p_r	=	peak reflection pressure
p_s	=	static pressure
p_w	=	wall pressure
p_0	=	stagnation pressure
$\boldsymbol{U}$	=	velocity vector
W_s	=	shock wave speed
$W_{s,m}$	=	shock wave speed measured by spherical probe
(x_A, y_A, z_A); (x_B, y_B, z_B)	=	coordinates of transducer A, B, respectively
(x_C, y_C, z_C); (x_D, y_D, z_D)	=	coordinates of transducer C, D, respectively
$\Delta\boldsymbol{R}$	=	change in shock wave location on the spherical probe
θ	=	shock inclination with respect the local sensor (see Fig. 1)
φ	=	shock inclination with respect the spherical probe holder

Indices

1	=	region upstream of traveling shock wave
2	=	region downstream of traveling shock wave

I. Introduction

THE flowfield generated by a moving shock or blast wave is of critical importance in many applications. The problem of muzzle blast in U.S. Army crew areas is of particular significance. Multiple reflections of blast waves over solid surfaces can cause substantial overpressure behind them, which can be harmful to the crew. Human injuries can occur at blast strengths much lower than those that cause equipment damage. To assess the blast overpressure and noise-related health hazards, a better understanding of the phenomenon of blast wave reflections is needed. A better understanding, however, requires more accurate measurement of pressure behind blast waves, which may have been reflected by irregular surfaces. The task of this study is to develop and test a probe that can measure the direction of shock or blast waves over the measurement location, as well as the pressure behind them.

Although pressure is a scalar quantity, its measurement is affected by the orientation of the probe in reference to the flow direction. This behavior is known as yaw or pitch response of the probe, which can seriously limit the accuracy of the measurements. Figure 1 shows a schematic of the probe orientation in reference to the flow velocity vector $\boldsymbol{U}$. If $\boldsymbol{n}_p$ is the unit vector normal to the pressure-sensing surface of the probe pointing in the inward direction, then θ is the angle between $\boldsymbol{n}_p$ and the unit vector $\boldsymbol{n}_u$ of the velocity vector $\boldsymbol{U}$ measured in an anticlockwise direction. When θ is 0 deg, then the probe measures stagnation pressure p_0. When θ is $\pm$90 deg, the measured pressure is reasonably close to the local static pressure of the flow p if the flow disturbance caused by the probe is ignored. For angles between 0 and 90 deg, the probe measures pressure between p_0 and p. Very often, in incompressible flows, the measured pressure p varies as $\cos\theta$.

Because, in the present case, the flow is induced by a moving shock or blast wave, the direction of the flow velocity coincides with the direction of the shock speed W_s. In that respect, the angle θ between $\boldsymbol{n}_p$ and $\boldsymbol{n}_u$ is also the angle between $\boldsymbol{n}_p$ and $\boldsymbol{n}_s$, where $\boldsymbol{n}_s$ is the unit vector normal to the shock surface (Fig. 1).

The objective of the present paper is to demonstrate and document the performance of a custom-designed probe that is capable of measuring the direction of the shock wave motion, as well as the overpressure behind. The probe has been tested in a large-scale shock-tube facility and in the field. The data obtained have been also compared with computational fluid dynamics (CFD) simulations of the flow over the probe. Section II of the paper describes the directional response of a single pressure transducer to a moving shock wave, and Sec. III describes the design characteristics of the new probe. Section IV documents evaluation tests made in the shock tube that demonstrate the directional response of the probe. Detection of the shock wave direction is described in Secs. V and VI, and results are discussed in Sec. VII. CFD results and comparison with experiment are presented in Sec. VIII. Uncertainties and limitations of the probe's capabilities are discussed in Sec. IX.

II. Directional Response of a Single Pressure Transducer

To demonstrate the yaw response of a typical high-frequency response pressure transducer at constant Mach number, several experiments were carried out in the shock-tube research facility described

Received 23 February 2002; revision received 27 September 2002; accepted for publication 8 October 2002.

*Professor, Experimental Aerodynamics and Fluid Mechanics Laboratory, Department of Mechanical Engineering. Associate Fellow AIAA.

†Graduate Research Assistant, Experimental Aerodynamics and Fluid Mechanics Laboratory, Department of Mechanical Engineering.

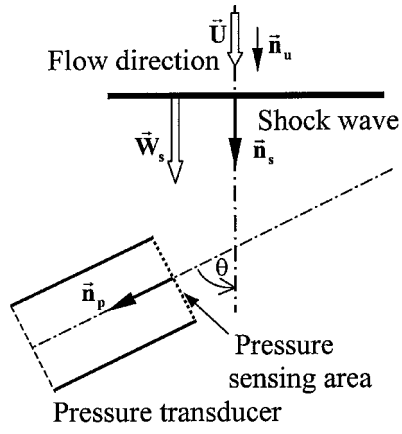

Fig. 1 Schematic of yaw response of pressure transducer to shock wave and flow direction.

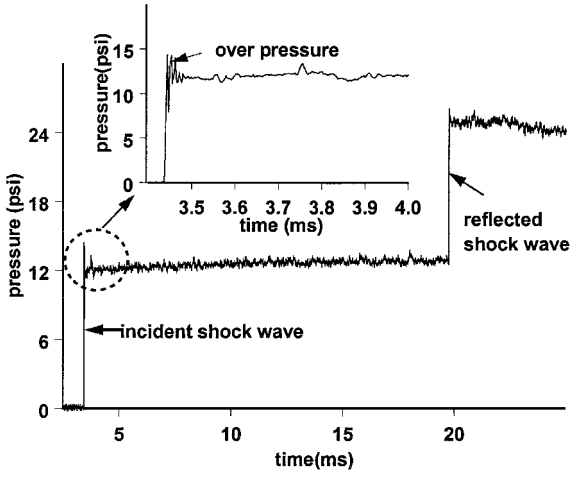

Fig. 2 Typical pressure signal of a single pressure transducer at $\theta = 0$ deg.

by Briassulis et al.[1,2] This facility has been used to better understand shock wave interactions with turbulent flows.[3]

Kulite pressure transducers, Type XCS-062-50D, were used in this investigation. The outside diameter of these transducers is about 1.2 mm, whereas the diameter of the sensing area is 0.7 mm. A stainless-steel holder was fabricated to house the transducer, the four leads, and the temperature-compensating unit in place so that the whole arrangement was made airproof.

In the experiments, the shock wave speed W_s was kept constant in direction and magnitude, and the probe's orientation was adjusted from outside the shock tube through the excess protruding holder length.

Two Kulite pressure transducers were also used to monitor the wall pressure below the pressure probes at a distance of 6 in. (152.4 mm) upstream. This pressure also served as a reference pressure because it was kept constant in all experiments. A third pressure transducer was placed further upstream to provide the triggering signal for the data acquisition. Thus, six pressure transducers were used in each experiment. All signals were low-pass filtered at 100-kHz cutoff frequencies and amplified by EC&G PARC preamplifiers and signal conditioners before they were digitized at a 500-kHz rate.

Figure 2 shows a typical pressure signal of the probe at $\theta = 0$ deg orientation to the flow and the shock wave direction. The passing of the incident shock wave produces the first jump in pressure, whereas the passing of the reflected shock off of the end wall of the shock tube produces the second jump in pressure.

One typical characteristic of probes like the present one is the overshot at the arrival of the incident shock. This is caused by a partial reflection of the incident shock over the transducer area that causes an overpressure level that depends on the size of the probe and the shock strength or its Mach number. The present probe is not immune to this behavior. The data shown in Fig. 2 indicate an overpressure of the order of 18–20% of the measured pressure sometime after this disturbance has subsided. The time-expanded pressure signal shown in the insert of Fig. 2 indicates a dumped oscillation of the pressure triggered by the shock, which is also known as transducer ringing.

One conclusion that can be drawn from the present tests is that this overpressure sensed by the Kulite pressure transducer is much lower than the pressure measured by PCB-type transducers. The report by Walton[4] describes substantial pressure overshoots for the 5-mm-diam PCB-type transducers. This temporary overpressure has been attributed to reflection of the incident shock off of the sensing surface of the transducer. An ideal reflection of a shock wave with Mach number $M_s = 1.26$, for instance the present one, over an infinite flat surface can produce an overpressure of 2.74 times the static pressure before the reflection. However, in the present case, the area of reflection is extremely small, its diameter is only 1.2 mm. Therefore, the overpressure due to this type of reflection over a finite surface is expected to be much smaller than the value predicted by the reflection theory over infinite flat surfaces. The reason for this behavior is that considerable "leakage" or "venting" of pressure takes place after the shock reflection off of the sensing area of the transducer. In fact, the present experimental data do confirm that. If the present transducers were measuring a full-scale reflection, then the overshoot of pressure immediately after the arrival of the incident shock should be about the same as the pressure behind the reflected shock over the end wall of the shock tube,[5,6] which is about 25.57 psig (176.3 kPa). If one considers that there are some viscous losses associated with the reflection, the measured value of 24.9 psi (171 kPa) behind the reflected shock off of the end wall of the shock tube is, within the experimental uncertainty, very close to the expected value. This measured pressure has to be compared with the peak overpressure immediately after the passage of the incident shock, which is about 14.6 psi (100.6 kPa). Thus, it is very reasonable to conclude that subminiature pressure transducers with small sensing areas, like the ones used in this investigation, exhibit reduced effects of shock reflections.

The directional effects of the single transducer probe are summarized in Figs. 3a and 3b, where the results of two different

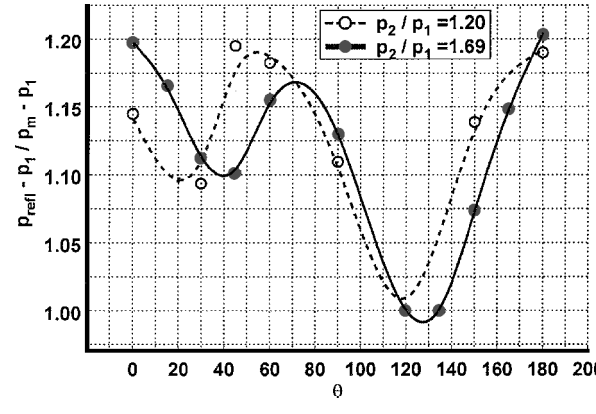

Fig. 3a Measured reflected pressure for various local yaw angles.

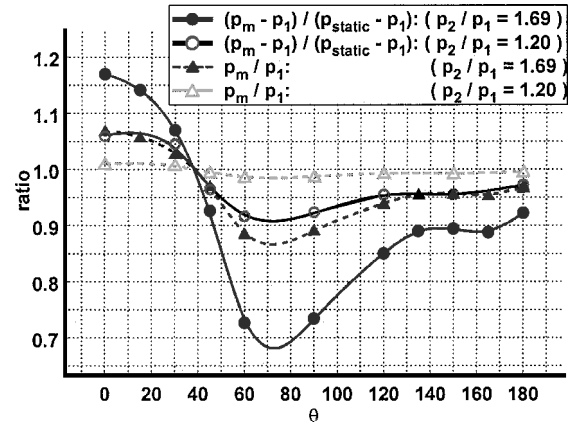

Fig. 3b Measured pressure ratio for various local yaw angles.

experiments are plotted. In the first experiment, the pressure ratio p_2/p_1 was 1.69, whereas in the second $p_2/p_1 = 1.20$. Figure 3a shows the measured peak reflected pressure at the arrival of the incident shock wave for various yaw angles θ of the probe. Pressure data are referenced to p_1, which is the ambient atmospheric pressure. The plotted data $p_{\text{refl}} - p_1$ are normalized with $p_m - p_1$, which is the measured pressure immediately after the peak where the effects of shock reflections and/or transducer ringing have subsided. A value of the plotted pressure ratio close to one indicates that there are no substantial effects due to shock reflections over the sensing area.

In the case of $p_2/p_1 = 1.69$, the measured reflected pressure tends to decrease with increasing θ up to 50 deg. At about $\theta = 60$ deg, the reflected pressure increases substantially. Our theoretical analysis and preliminary CFD work suggest that this is most probably due to the transition from regular reflection to Mach reflection[4] and the appearance of both the triple point and the Mach stem. At $\theta > 60$ deg, the measured pressure drops substantially, indicating smaller contributions from shock reflection effects. No shock reflection effects appear to be present in measured pressure for $135 > \theta > 100$ deg. However, at $\theta = 150$, 165, and 180 deg, substantial overpressure was observed. There are two possible explanations for this overpressure. The ringing of the transducer may be the first one. The second is related to the design of the cavity that houses the sensing area. Part of the shock wave may travel within the cavity in a direction opposite to the direction of the main shock motion and possibly produce a weak reflection with the small sensing area.

In the case of pressure ratio $p_2/p_1 = 1.2$, which corresponds to weaker shocks with $M_s = 1.08$, a behavior similar to that in the higher-pressure ratio case can be observed. No reflection was observed at $\theta = 120$ deg.

Because the strength of the shock wave was kept constant, the pressure behind the shock in all experiments was also reasonably constant with time. This provided the opportunity to obtain pressure measurements in the absence of effects related to shock reflections and transducer ringing. Figure 3b shows the measured pressure p_m obtained immediately after the passing of the shock after shock reflection and oscillations due to ringing have subsided. The data are normalized by the measured static pressure at the wall pressure p_w. At $\theta = 0$ deg, the probe measures the total pressure p_{02}. The data show a ratio of $p_m/p_w = 1.06$ for the high-pressure ratio case, which is close to the theoretical value $p_{02}/p_2 = 1.097$ for $M_2 = 0.359$. The measured pressure starts to decline as θ increases, and it reaches a minimum between $\theta = 60$ and 90 deg. In the range $90 < \theta \leq 180$ deg, the probe seems to measure the static pressure of its wake, which is characteristic of the backpressure behind a reasonably thin bluff body.

The main conclusions of the single pressure transducer tests are as follows:

1) Subminiature piezoresistive pressure transducers, because of their small size, exhibit fewer effects due to shock reflections off of their sensing area than traditional piezoelectric PCB-type transducers.

2) Strong directional effects are associated with these probes.

III. Four Pressure Transducer Spherical Probe

The information described in the preceding section was used to design a probe that could detect the direction of blast or shock wave, as well as the pressure behind it. The functional relation between the measured pressure p_m in the case of a single transducer and the flow or shock direction θ, as shown in Fig. 3b, is complicated. The existence of several inflectional points makes the functional relation not unique: For a given value of the pressure ratio p_m/p_w, there might be more than one corresponding value of the angle θ. This problem may be overcome by using more than one pressure transducer in a proper configuration. In the proposed new design, four Kulite pressure transducers were used that were mounted on specific locations on the surface of a 1-in. (25.4-mm)-diam brass sphere.

Figure 4 shows a schematic of the probe with the locations of the transducers. The probe was fabricated by machining the inside of a brass sphere so that adequate space is provided for the pressure transducers and their leads.

One pressure sensor was mounted on the furthest upstream tip of the sphere, whereas the other three were mounted on a Y configuration on a plane perpendicular to the probe holder plane and to the axis of symmetry of the first sensor. The pressure transducers used were specially fabricated by Kulite and had specifications close to Type XCS-062-10D sensors. The lack of adequate space within the 1-in. sphere, which was needed to accommodate all of the accessories of the transducers, led to a design with the temperature-compensating unit 24 in. (609.6 mm) away from the sensors, outside the sphere.

The diameter of the sphere was chosen to be the smallest possible, which will allow for meaningful determination of shock's traveling time/distance and for adequate space internally to accommodate all pressure transducers and their accessories. Ideally, a zero diameter would provide information on a point measurement of pressure. However, this is not practical for the reasons explained earlier. In addition, the finite size of the probe provides a finite distance between the transducers, which is used to estimate the shock speed W_s from the shock flight time information between the transducers.

IV. Tests and Directional Response

The newly fabricated spherical probe was mounted on the shock tube for testing. The experimental arrangement was similar to that described in Sec. II. One pressure transducer was located at the wall below the probe, and one was located upstream of the probe and was used to trigger the data acquisition. An additional single Kulite transducer, located downstream of the sphere, was also used to measure the pressure inside the flow.

The spherical probe was yawed on the horizontal plane by a mechanism similar to that used in the case of the single transducer tests. In the present case, however, the yaw angle φ, which represents the rotation of the probe about its vertical axis, does not always coincide with the angle θ between the individual pressure transducers and the shock wave as it has been defined in Fig. 1. For transducer B, for instance, it is always $\theta_B = 90$ deg because $\boldsymbol{n}_B$ is normal to the plane of yaw rotation and, therefore, it is independent of φ. For transducer D, it is always $\theta_D = \varphi$ and for transducers A and C it is

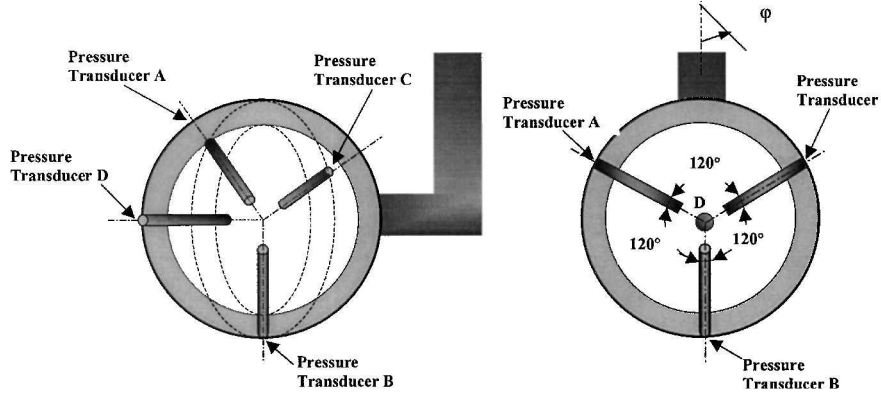

Fig. 4 Spherical probe with four Kulite pressure transducers.

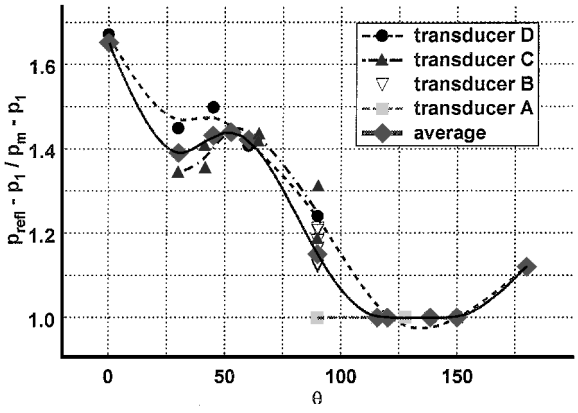

Fig. 5 Reflected pressure measured by spherical probe for $p_2/p_1 = 1.45$.

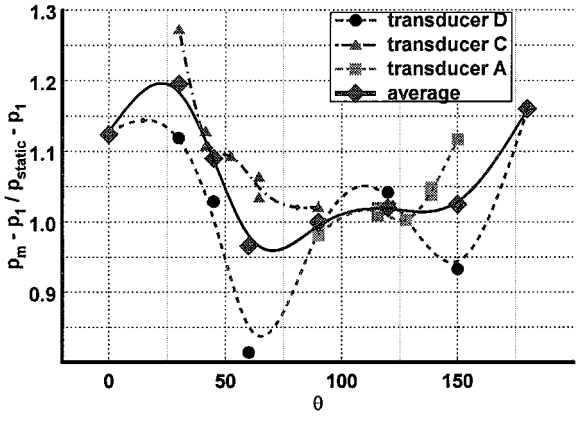

Fig. 6 Pressure measured by spherical probe for $p_2/p_1 = 1.45$.

$\theta_A = f_1(\varphi)$ and $\theta_C = f_2(\varphi)$, where $f_1(\varphi)$ and $f_2(\varphi)$ are geometrical functions relating φ and θ.

The data shown in Figs. 5 and 6 have been obtained at $p_2/p_1 = 1.45$. Figure 5 shows the directional effects of the spherical probe. The data obtained from each of the four transducers have been plotted in Figs. 5 and 6. Because of existing symmetries, more than one data point, obtained by different transducers, may correspond to the same angle θ. In Fig. 5, the peak reflected pressure $p_{refl} - p_1$ has been normalized by the pressure $p_m - p_1$, measured immediately after all disturbances associated with shock reflections and transducer ringing have subsided.

One significant feature of this probe is that shock reflections, whenever they exist, are greater than that in the case of a single transducer. For instance, at $\theta = 0$ deg, the value of 1.66 has been obtained for the pressure ratio $(p_{refl} - p_1)/(p_m - p_1)$. This value is substantially greater than the value of 1.198 shown in Fig. 3a for a slightly higher pressure ratio $p_2/p_1 = 1.69$ but lower than the value expected after a reflection of the shock off of an infinite flat surface. The theoretical value of p_{refl}/p_1 behind a one-dimensional reflection appears to be 1.42, which results in $(p_{refl} - p_1)/(p_m - p_1) = 2.07$, a value that is about 25% greater than the experimental value of 1.66. The present data, obtained with the spherical probe, indicate that the problem of shock reflection is less acute than in the case of PCB transducers but significantly greater than in the case of a single transducer.

It appears that the sphere, as a solid surface surrounding the pressure transducer, prevents an early "leakage" of pressure from occurring after the reflection by delaying the onset of two-dimensional effects. This seems to explain why shock reflections are more evident in the case of the spherical configuration than in the case of a single isolated transducer.

As the angle θ increases, the reflected pressure decreases. At about $\theta = 50$ deg, p_r increases locally due to the transition from regular to Mach reflection.[7] It then decreases further as θ increases. At $\theta = 90$ deg, only transducer A shows no evidence of shock reflections. All other transducers indicate that shock reflection effects are present at this angle. Transducer A shows no or very few effects of shock reflections, most probably because it is always positioned in the wake of the sphere. A spline-fit curve over all points, locally averaged, indicates a strong similarity with the behavior of the single transducer probe shown in Fig. 3a.

Figure 6 shows the pressure ratio $p_m - p_1/p_{static} - p_1$ dependence on the flow direction in the case of the spherical probe. There is some considerable scatter of the data in regions of overlapping values of θ. An average, spline-fit curve has also been drawn to better indicate the overall trend. The data show that, at $\theta = 90$ deg, the measured pressure p_m is very close to the static.

V. Detection of Shock Wave Direction

The time-dependent signals of the four transducers A, B, C, and D, that are mounted on the sphere at different locations can provide us with the exact time the shock reaches each of the four transducers. Thus, the time differences of the shock arrivals among them can be estimated. Because the distance between any two of these transducers is known, the shock velocity can be determined by estimating the "flight" time of the shock from one transducer to the next. If the shock wave foot on the sphere changes position by $\Delta\boldsymbol{R}$ within time Δt, then the shock speed vector can be estimated from $\boldsymbol{W}_s = (\Delta\boldsymbol{R} \cdot \boldsymbol{n}_s)/\Delta t$. The position traveled $\Delta\boldsymbol{R} \cdot \boldsymbol{n}_s$ is assumed to be in the direction normal to the shock $\boldsymbol{n}_s$. It can be expressed in terms of nonorthogonal components as $\Delta\boldsymbol{R} \cdot \boldsymbol{n}_s = f(\Delta R_1, \Delta R_2, \Delta R_3)$, where ΔR_1, ΔR_2, and ΔR_3 are the projections of the vector $\boldsymbol{n}_s$ on the known directions defined between one of the four pressure transducers and the remaining three. If $\Delta R_2/\Delta R_1 = a$ and $\Delta R_3/\Delta R_1 = b$, then in matrix notation,

$$\|L\| \begin{Bmatrix} n_1 \\ n_2 \\ n_3 \end{Bmatrix} = \begin{Bmatrix} 1 \\ a \\ b \end{Bmatrix} k \qquad \text{or} \qquad \begin{Bmatrix} n_1 \\ n_2 \\ n_3 \end{Bmatrix} = \|L\|^{-1} \begin{Bmatrix} 1 \\ a \\ b \end{Bmatrix} k$$

where $\|L\|$ is the directional matrix defined as

$$\|L\| = \begin{bmatrix} x_C - x_D & y_C - y_D & z_C - z_D \\ x_A - x_D & y_A - y_D & z_A - z_D \\ x_B - x_D & y_B - y_D & z_B - x_D \end{bmatrix}$$

and $k = \Delta R_1$.

The transducer locations are known, and the ratios a and b can also be determined by the time differences. Thus, the unit vector $\boldsymbol{n}_s$ can be estimated. A more detailed description of the method of calculating the shock wave direction is provided in Ref. 8.

The present approach involves two assumptions. First, it is assumed that there is no speed variation of the shock front during the time it travels from one transducer to the other. Second, it is assumed that the shock remains locally flat within a distance of 1 in., which corresponds to the diameter of the spherical probe. Both assumptions are reasonable and they worked very well within the context of the present work.

VI. Description of Computational Algorithm

Based on the background theory described earlier, a computational algorithm was devised, prescribed, and demonstrated. The algorithm can carry out the following tasks:

1) Detect the shock wave and its arrival time at the locations of the four transducers.

2) Estimate the shock direction and its speed.

3) Estimate the pressure rise after the passage of the shock wave.

The following methodology was used to detect the passage of shock wave, for which groups of six consecutive digital points were considered:

1) A continuously increase in pressure should be detected on all six points.

2) The summation of all pressure increments from point to point should be above a given threshold T_{h_1}:

$$\Delta p_{21} + \Delta p_{32} + \Delta p_{43} + \Delta p_{54} + \Delta p_{65} \geq T_{h_1}$$

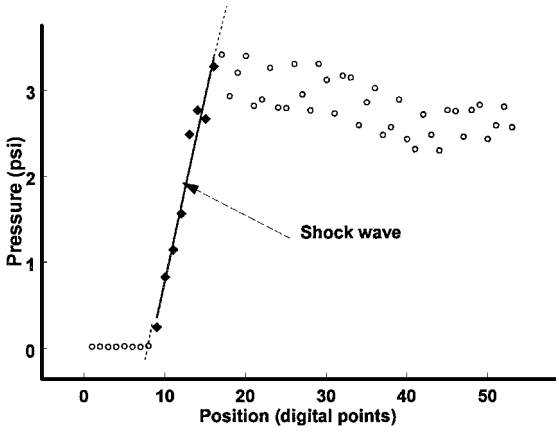

Fig. 7 Shock detection algorithm.

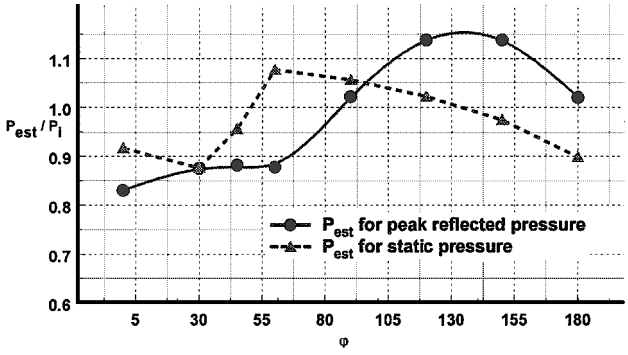

Fig. 8 Estimators performance for peak reflected pressure and static pressure.

The threshold level T_{h1} was determined as a fraction of the difference between the maximum and minimum pressure in a given data file.

If the preceding condition is satisfied, then a shock wave may exist in this group of six points. Subsequently, a least-square fitting of a linear equation with six data points was used to estimate the maximum slope of pressure signal rise due to the passage of the shock and its arrival time (Fig. 7). The shock wave direction and speed were determined by the use of the mathematical formulation described in the preceding section. With knowledge of the direction of the shock wave $\boldsymbol{n}_s$ in relation to the transducer normal vector $\boldsymbol{n}_A$, $\boldsymbol{n}_B$, $\boldsymbol{n}_C$, or $\boldsymbol{n}_D$ in terms of angle θ_A, θ_B, θ_C, or θ_D, the pressure behind the shock was estimated in various ways. The first estimate can be obtained from the relation between the pressure ratio p_2/p_1 across the shock and its Mach number M_s, $(p_2/p_1) = 1 + [2\gamma/(\gamma+1)](M_s^2 - 1)$, where M_s is known from the measured W_s and the local sound speed. More estimates can be obtained from the measured direction of the shock and the available directional response information as shown in Figs. 5 and 6 after normalization by averaging the pressure over the values of four transducers:

$$P_{av} = \tfrac{1}{4}[p_A(\theta_A) + p_B(\theta_B) + p_C(\theta_C) + p_D(\theta_D)]$$

Another estimate of the static pressure behind the shock can be obtained by considering the estimator $p_{est} = \frac{1}{4}[p_A(\theta_A) + p_B(\theta_B) + p_C(\theta_C) + p_D(\theta_D)]$. By the use of the data shown in Fig. 6, the performance of this estimator has been assessed, and the results are plotted in Fig. 8 against the known shock wave inclination angle with respect the spherical probe φ. Values of $P_{est} = \frac{1}{4}[P_A(\theta_A) + P_B(\theta_B) + P_C(\theta_C) + P_D(\theta_D)]$ have been computed from the existing data, where each of the $P_A(\theta_A)$, $P_B(\theta_B)$, $P_C(\theta_C)$, or $P_D(\theta_D)$ is the corresponding pressure ratio $(p_m - p_1)/(p_{static} - p_1)$. Values of P_{est} have been normalized by the true values of the ratio P_i shown in Fig. 6. Similar procedures have been applied to evaluate an estimator for the peak reflected pressure based on averaging the pressure over the four transducers. In this case, the data shown in Fig. 5 for the pressure ratio $(p_r - p_1)/(p_m - p_1)$ have been used. The results are also shown in Fig. 8. It appears that this estimator could recover the true value of the pressure ratio to within 10% error in the case of static pressure and within 15% error in the case of the peak reflected pressure. This performance can be considered rather satisfactory if it is compared to the performance of an estimator based on information based on one pressure transducer, which is the case of the data shown in Figs. 5 and 6. These data show that an estimate based on information from one pressure transducer can be in error by $\pm 34\%$ in the case of peak reflected pressure, or by $\pm 20\%$ in the case of static pressure. Thus, the four-transducer estimator reduces the uncertainties involved in the one-transducer estimator by more than 50%. In combination with some other information, the four-transducer estimator can yield results with uncertainty much lower than the values just cited.

VII. Results and Discussion

The algorithm and the associated software package were tested with real signals obtained in the yaw response tests of the spherical probe. Figure 9 shows the results of the tests, which were carried out to evaluate the performance of the algorithm and the probe. The difference between the measured angle φ_m and the nominally known value of the shock wave direction φ, $\Delta\varphi_m = \varphi_m - \varphi$ is plotted against φ. The percentage difference $\Delta\varphi_m/\varphi = (\varphi_m - \varphi)/\varphi \times 100$ is also plotted in Fig. 9. At small values of φ, the difference is 0.2 deg, whereas at large values of φ, the difference is, on average, about ± 6.5 deg. Note that the estimated values of φ_m are within 5% of the nominal values of φ.

A comparison of the results between the data obtained with the spherical probe and those obtained with a single transducer is shown in Fig. 10a. The values at small angles φ suggest higher p_r in the case of the spherical probe than in the case of a single isolated transducer. Mach reflections take place at about 50–60 deg in both cases. The directional response is also quite similar for $\theta > 60$ deg.

A comparison between the spherical probe and the single probe in the measurement of the pressure after the effects of shock reflection and transducer ringing have subsided is shown in Fig. 10b. There is a considerable similarity in the directional sensitivity between the two probes. However, it appears that the values measured by the spherical probe may be overestimated.

Figure 10c shows the ratio of the shock speed measured by the spherical probe $W_{s,m}$ to that of the undisturbed shock velocity measured by the wall pressure transducers W_s against the measured angle φ_m of the direction of the moving shock. The data in Fig. 10c indicate that the two measured values of the shock velocity agree reasonably well with each other. The two data sets of measured velocity appear to be within 10% from each other for shock angles in the range of 0–90 deg. The difference between the two measured values of shock speed increases at larger angles φ_m and reaches a value of about 22% at angles close to 180 deg. This deterioration of the performance of the probe is most probably due to the interference of the probe holder with the incoming shock. Overall, it

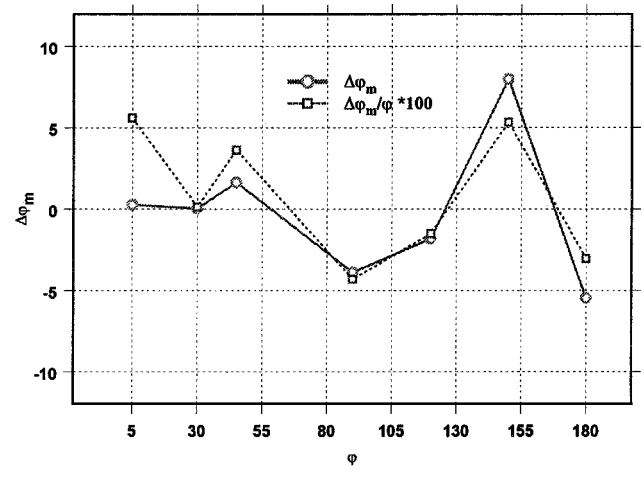

Fig. 9 Comparison between measured shock wave direction φ_m and nominal shock wave direction φ ($\Delta\varphi_m$ is defined as $\Delta\varphi_m = \varphi_m - \theta\varphi$).

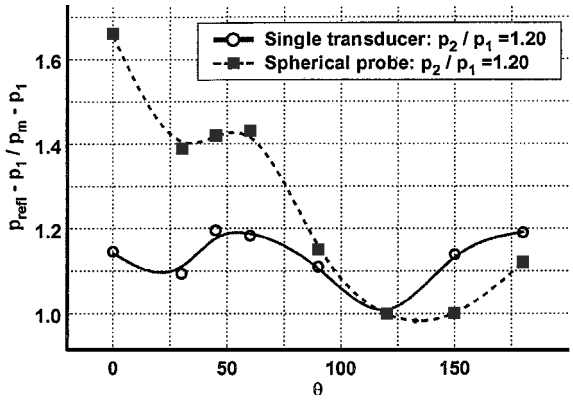

Fig. 10a Comparison between single pressure transducer and spherical probe: case of peak reflected pressure.

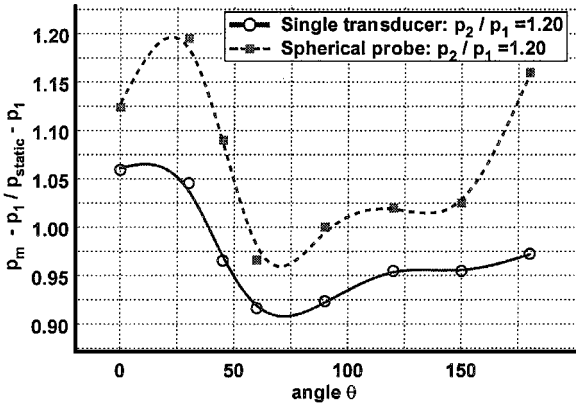

Fig. 10b Comparison between single pressure transducer and spherical probe: case of mean pressure.

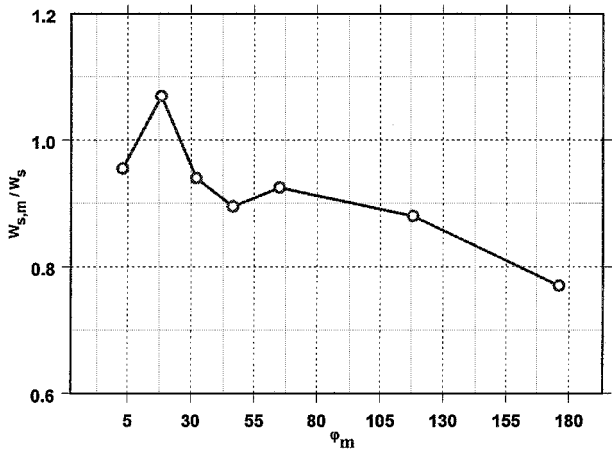

Fig. 10c Comparison of measured shock velocity by spherical probe $W_{s,m}$ and actual undisturbed shock velocity W_s measured by wall pressure transducers.

appears that the spherical probe underestimates the shock velocity, on average, by about 12%.

VIII. Physical Characteristics

To obtain insight into the physical processes involved in the interaction between a moving shock wave and a solid sphere, the commercially available CFD software package FLUENT was used to obtain a numerical solution of the unsteady Euler equations in an axisymmetric formulation. In the present case, as is the case with most shock wave capturing numerical schemes, the thickness of the shock wave is considerably overestimated. This shortcoming, however, does not preclude the use of CFD in understanding the basic physics of the interaction between a moving shock and its induced flow with a sphere. In fact, the present CFD package yielded almost identical results in terms of shock thickness as those obtained by more advanced algorithms.[9]

Figure 11 shows the evolution of the pressure field during the interaction obtained in the case of shock strength with $p_2/p_1 = 1.45$. At the beginning of the interaction, as the shock impinges on the sphere at its most upstream region, a reflected shock propagating in the opposite direction starts to develop. The incident shock starts to propagate around the surface of the sphere. At the same time, regular reflections occur that propagate radially upward and in the upstream direction. Thus, a compressive pattern of variable strength appears to be developing in the first guardant of the sphere as a result of the incident shock reflection over the surface of the sphere and the forward motion of the shock. At an angle of about 45 deg from the leading-edge radius, Mach reflection seems to take place. In this region, the shock foot propagates faster than the shock front. At 90 deg, the shock foot has the same speed as the shock front. At angles greater than 90 deg, the shock foot starts to slow down relative to the shock front. Expansion waves are formed after the shock wave passes the top point of the sphere at 90 deg from the leading edge and a lower pressure region in the vicinity of the surface of the sphere develops. As the shock wave leaves the sphere, a recompression of the flowfield occurs in the wake region close to the symmetry line, which starts to propagate upstream.

As a result of Mach reflections at angles between 0 and 45 deg and expansion waves at angles between 135 and 180 deg, there is an apparent speed up or slow down of the shock foot at the surface of the sphere, respectively, in relation to the motion of the undisturbed shock front far away from the sphere. The question is how this behavior affects the detection schemes of the shock passage. The diffraction theory of Bryson and Gross[7] has been adopted in the present case of weak shock to provide an estimate of the difference in the propagation speed of the shock foot and the undisturbed shock front. This theory indicated that the shock foot propagates faster by about 10% in the first quadrant of the sphere than the shock front and that it is slower by about the same amount in the second quadrant.

The present CFD results indicated that the effects of the shock foot slow in the second quadrant of the sphere, and they persist for some time downstream in the wake of the sphere. At the moment the undisturbed shock front is at the trailing edge of the sphere, it has traveled a distance of $2R$ over the projection of the circumference of the sphere. At the same time, the shock foot has traveled a longitudinal distance of $1.8R$, where R is the radius of the sphere. Thus, an estimated relative slow down of the shock foot velocity of $\Delta W_s / W_s = 0.10$ may have occurred. This estimate appears to be in agreement with the measurements shown in Fig. 10c.

A comparison between the computed and measured time-dependent signals is shown in Figs. 12a and 12b. Figure 12a shows the comparison of the two signals obtained at the leading edge of the spherical probe. The computed signal follows the experimental one reasonably well. The peak overpressure at the onset of the shock impact that is related to its reflection over the probe surface appears to be slightly lower than the measured one. The measured signal, however, indicates a transducer ringing due to high-frequency resonance, which produces high-amplitude oscillations. The computed pressure ratio $(p_{\text{refl}} - p_1)/(p_m - p_1)$ appears to be 1.44, a value that is about 12% lower than the measured one 1.65 (see also Fig. 5). In that respect, the agreement between the two signals may be considered satisfactory. At times after the transducer ringing effects have decayed, the computed signal is slightly higher than the measured pressure signal.

A comparison of the two pressure signals at 90 deg is shown in Fig. 12b. The peak reflected pressure ratio $(p_r - p_1)/(p_m - p_1)$ computed by our inviscid model is 1.19, whereas the measured value of this ratio is 1.225.

The rather good agreement between the experimentally obtained pressure data and those obtained by inviscid CFD analysis provides a certain confidence on the accuracy and consistency of the present experimental results. It also indicates that CFD analysis can be useful in revealing some of the physics of the flow under consideration within the context of its limited validity and assumptions.

Further insight into the physics of the pressure field can be obtained by considering that the flow is really viscous and that a

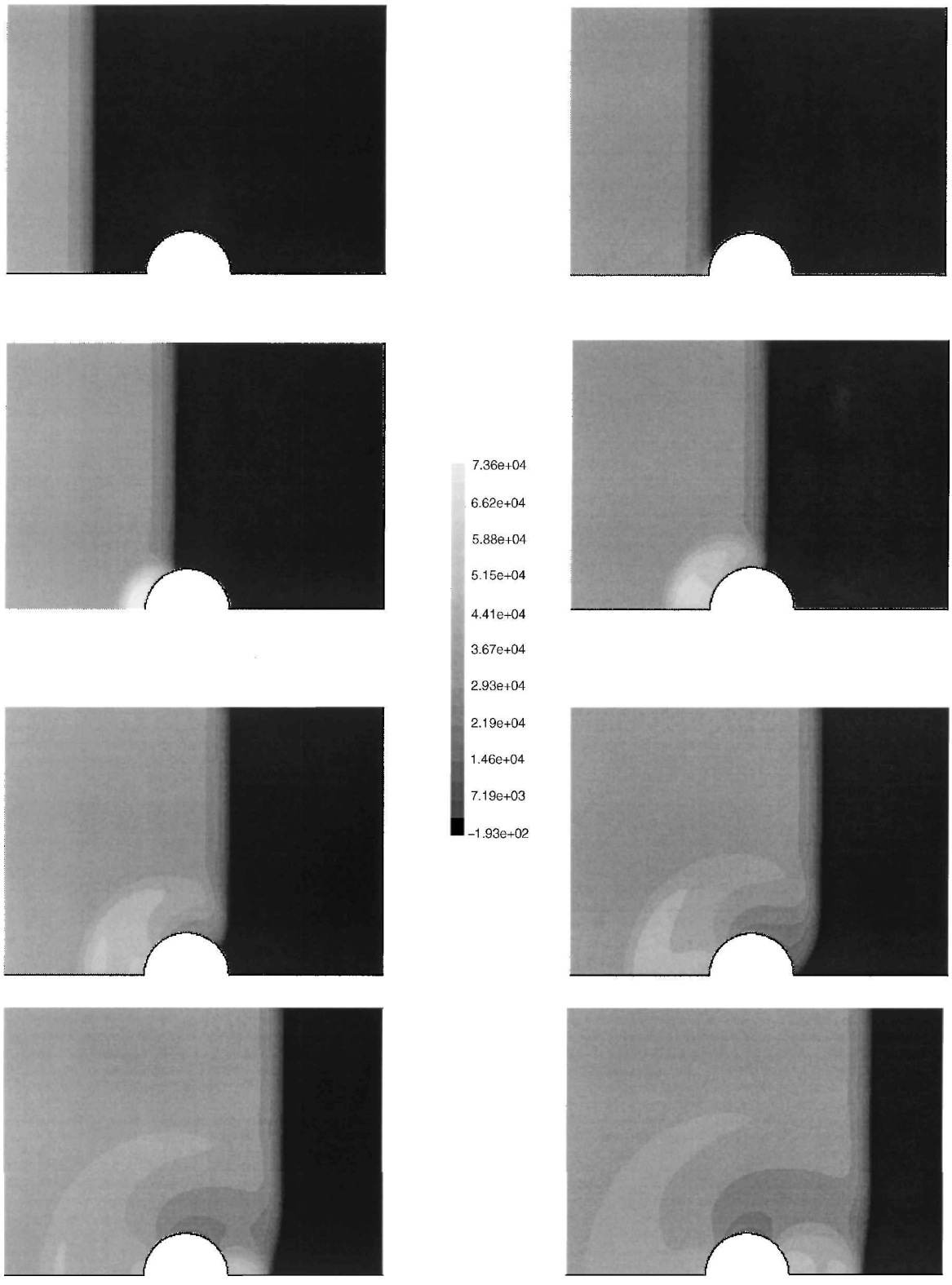

Fig. 11 Pressure field obtained by CFD for $p_2/p_1 = 1.45$.

turbulent subsonic boundary layer is developing over the surface of the spherical probe behind the moving shock. Although the pressure is a local quantity, it contains contributions from the entire flowfield. This can easily be seen by considering the transport equation for dilatation S_{kk} (Ref. 3):

$$\frac{\mathrm{D}(S_{kk})}{\mathrm{D}t} = -S_{ik}S_{ik} + \frac{1}{2\Omega_k\Omega_k} + \frac{1}{\rho^2}\frac{\partial\rho}{\partial x_k}\frac{\partial p}{\partial x_k} - \frac{1}{\rho}\frac{\partial^2 p}{\partial x_k \partial x_k} + \frac{\partial}{\partial x_k}\frac{1}{\rho}\frac{\partial \tau_{kq}}{x_q}$$

where Ω_k is the vorticity and S_{ik} is the rate-of-strain tensor. Solving for the pressure term, we can obtain the compressible flow version of Poisson's equation, which, in principle, can be integrated over the entire flowfield to yield the local pressure. Thus, contributions from the shock foot and those from the undisturbed shock are integrated, and it is rather difficult to differentiate between them. In addition, the probe, due to its limited spatial resolution, can not resolve accurately the pressure within the moving shock, let alone distinguish the effects of a slightly curved shock foot.

The pressure gradient that is associated with the moving shock is also expected to generate a large amount of vorticity flux at the

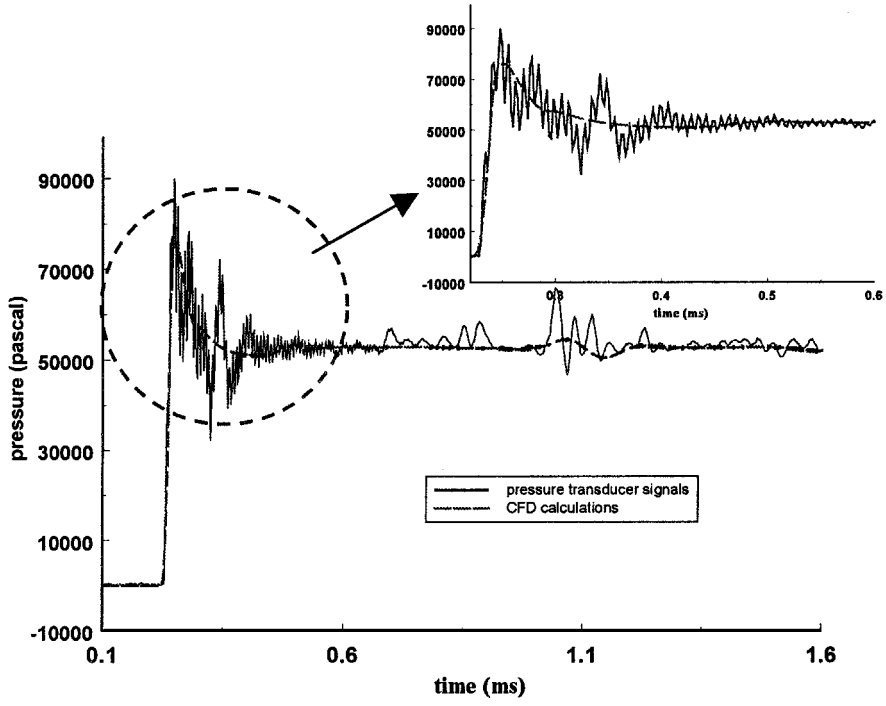

Fig. 12a Comparison between measured and computed pressure signals at the leading edge of the spherical probe.

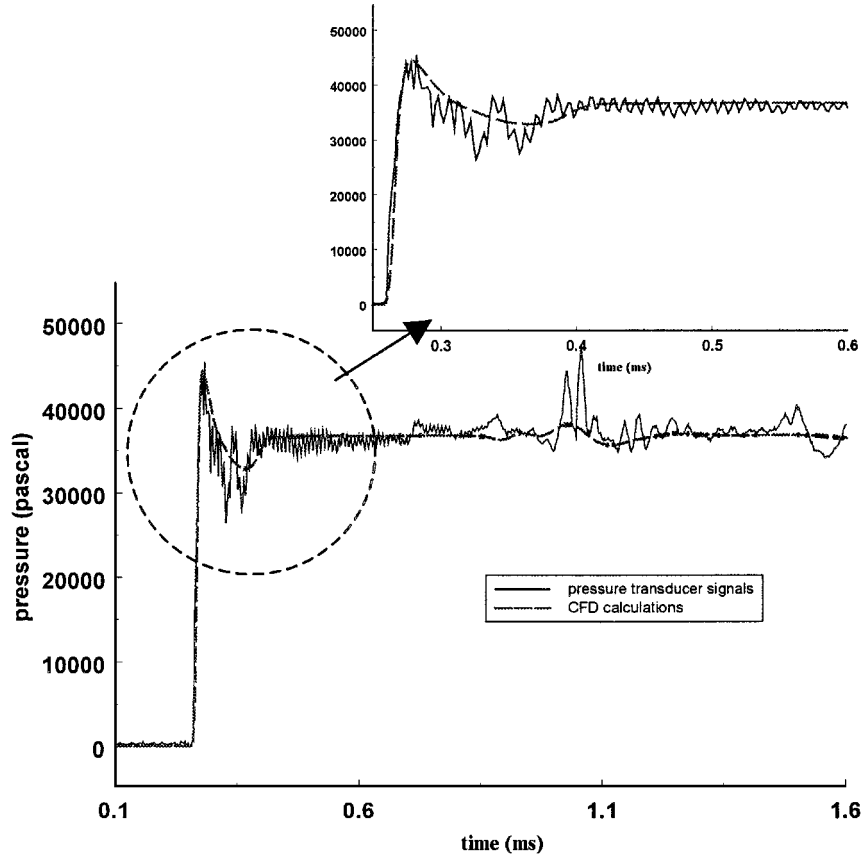

Fig. 12b Comparison between measured and computed pressure signals at the top of the spherical probe.

solid surface of the sphere. Subsequently, it enters the flowfield. The momentum equation evaluated at the wall beneath any flowfield because of no-slip conditions yields[10]

$$\frac{\partial p}{\partial x_i} = -\mu \varepsilon_{ijk} \frac{\partial \Omega_k}{\partial x_j}$$

Thus, the large pressure fluctuations shown in the measured pressure signals of Figs. 12a and 12b may be a result of strong vortical motions associated with the flow structures generated immediately behind the moving shock, which carry large amounts of vorticity produced by the no-slip conditions at the wall and the pressure gradient parallel to the wall.

IX. Uncertainties Involved

The uncertainties involved in the measurements of the shock speed and its direction are determined by the sampling frequency and the resolution of the analog-to-digital converters (ADCs). The ADCs used had a 14-bit resolution and the data were sampled at

a 500-kHz sampling rate. Thus, the resolution in time was 2 μs, whereas the resolution in amplitude was $\pm 5\ \mathrm{V}/2^{14} = 0.6$ mV/bit.

The uncertainty in estimating the shock velocity $W_s = \Delta R/\Delta t$ can be obtained from

$$\Delta W_s/W_s = \{[\Delta(\Delta t)/\Delta t]^2 + [\Delta(\Delta R)/\Delta R]^2\}^{\frac{1}{2}}$$

where $\Delta(\Delta t)$ is the uncertainty in estimating time, 2 μs, $\Delta(\Delta R)$ the uncertainty in estimating shock position. For a typical shock with speed of 400 m/s, $\Delta(\Delta R) \cong 0.8$ mm. Under these rather extreme circumstances, $\Delta W_s/W_s \cong 0.09$. This estimate can be further reduced if a linear interpolation is used to detect the arrival of the shock more accurately than within one digital point. By the use of the interpolated value, the uncertainty in time will be reduced by 50%, which will also reduce the uncertainty in estimating W_s to $\Delta W_s/W_s \cong 0.05$.

The uncertainty in estimating the Mach number of the moving shock M_s, appears to be the same as in $\Delta W_s/W_s$ because $\Delta M_s/M_s \cong \Delta W_s/W_s$. The uncertainty in the measurements of the pressure behind the shock p_2 can be found from the relation

$$\frac{\Delta p_2}{p_2} = \frac{[4\gamma/(\gamma+1)]M_s^2}{1 + [2\gamma/(\gamma+1)]\left(M_s^2 - 1\right)} \frac{\Delta M_s}{M_s}$$

which yields a value of 0.101.

The corresponding uncertainty in the shock direction can be seen from the matrix relation

$$\begin{Bmatrix} n_1 \\ n_2 \\ n_3 \end{Bmatrix} = \|L\|^{-1} \begin{Bmatrix} 1 \\ a \\ b \end{Bmatrix} k$$

By differentiating the original matrix, we obtain

$$\begin{Bmatrix} \delta n_1 \\ \delta n_2 \\ \delta n_3 \end{Bmatrix} = \|L\|^{-1} \begin{Bmatrix} 1 \\ a \\ b \end{Bmatrix} \delta k$$

For example, when the shock arrives at the location of transducer D first, then the inverse matrix $\|L\|^{-1}$ becomes

$$\|L\|^{-1} = \begin{bmatrix} -0.6667 & -0.6667 & 1.3334 \\ 1.1547 & -1.1547 & 0 \\ -0.6667 & -0.6667 & -0.6667 \end{bmatrix}$$

Thus,

$$\delta n_1 = [-1 - a + 2b] \cdot 0.6667 \delta k$$

$$\delta n_2 = [1.1547 - 1.1547a] \delta k$$

$$\delta n_3 = [-1 - a - b] \cdot 0.6667 \delta k$$

Because $\delta k = 0.8/25 = 0.032$ in., for $\varphi = 5$ deg, where α is the rotation angle, $a = 1.0588$, $b = 0.9412$, and $\delta n_1 = 0.00376$. Thus, $\delta\alpha_1 = 0.043$, $\delta\alpha_2 = 0.025$, and $\delta\alpha_3 = 0.85$ deg. These are typical uncertainties associated with the detection of shock wave direction.

Although our CFD work was intended to provide qualitative information on the interaction of the moving shock with the spherical probe, a grid independence study was carried out to quantify the variations involved in the quantitative results. One run with twice the grid size and a second with one-half of the grid size indicated less than a 1% change in the pressure field detected over the probe.

X. Conclusions

A new probe has been designed, fabricated, and tested. This probe is capable of detecting the local direction of blast or moving shock waves, as well as their strength. The probe consists of a sphere, 1 in. (25.4 mm) in diameter, with four pressure transducers mounted on its surface. The direction of the moving wave can be determined by measuring the flight time of the shock between various pairs of pressure transducers. The probe is sensitive to the incoming shock and flow direction. Its directional response is, to a certain extent, similar to that of a single pressure transducer. However, the ability to determine the shock wave direction provides better estimates of the pressure measurements behind the shock. In that respect, the present probe maybe characterized as omnidirectional.

The probe performance has been assessed and validated in shock-tube tests, as well as in field measurements. The data obtained were also compared with CFD calculations with satisfactory results. These evaluation tests of the algorithm developed to detect the direction and strength of blast waves indicated that the direction could be estimated to within 5 deg of the true direction. No calibration is needed for the detection of the direction of the shock wave motion. Calibration of the probe is essential, however, if quantitative information on the pressure field is required. In this case, the pressure behind the moving shock could be determined by several methods to within a 10% uncertainty.

Acknowledgments

The authors acknowledge the financial support provided by the U.S. Army Research and Development Engineering Center, monitored by Henry Hudgins and Frank Drzewiecki. Patent application is pending.

References

[1] Briassulis, G., Agui, J., Andreopoulos, J., and Watkins, B. C., "A Shock Tube Research Facility for High-Resolution Measurements of Compressible Turbulence," *Experimental Thermal and Fluid Science*, Vol. 13, No. 4, 1996, pp. 430–446.

[2] Briassulis, G., Agui, J., and Andreopoulos, Y., "The Structure of Weakly Compressible Grid Turbulence," *Journal of Fluid Mechanics*, Vol. 432, 2001, pp. 219–283.

[3] Andreopoulos, Y., Agui, J. H., and Briassulis, G., "Shock Wave–Turbulence Interactions," *Annual Review of Fluid Mechanics*, Vol. 32, 2000, pp. 309–345.

[4] Walton, W. S., "Improvement of Air Blast Measurement, ILIRV Task 5," U.S. Army, Aberdeen Proving Ground, MD, 1981.

[5] Saad, W. A., *Compressible Fluid Flow*, Prentice–Hall, Englewood Cliffs, NJ, 1993, pp. 187–192.

[6] Whitham, G. B., *Linear and Nonlinear Waves*, Wiley-Interscience, New York, 1974, pp. 263–274.

[7] Bryson, A. E., and Gross, R. W. F., "Diffraction of Strong Shocks by Cones, Cylinders and Spheres," *Journal of Fluid Mechanics*, Vol. 10, No. 1, 1961, pp. 1–20.

[8] Andreopoulos, Y., "The New Blast Over Pressure Probe: Field Tests at Yuma Proving Grounds," Final Rept. DAAE30-01-M1245, U.S. Army Tank Automotive Research and Development Command/Armament Research, Development, and Engineering Center, Picatinny Arsenal, NJ, March 2002.

[9] Chang, S. C., Wang, X. Y., and Chow, C. Y., "The Space–Time Conservation Element and Solution Element Method—A New High-Resolution and Genuinely Multidimensional Paradigm for Soling Conservation Laws," NASA TM 1998-208843, 1998.

[10] Andreopoulos, J., and Agui, J., "Wall Vorticity Flux Dynamics in a Two-Dimensional Turbulent Boundary Layer," *Journal of Fluid Mechanics*, Vol. 309, 1996, pp. 45–84.

R. P. Lucht
Associate Editor